

Testing of a high temperature radiatively cooled Li/Ta heat pipe in Magnum-PSI



G.F. Matthews^{a,*}, R.E. Nygren^b, T.W. Morgan^c, S.A. Silburn^a, P.R. Cooper^a, R. Otin^a, A. Tallarigo^a, the Magnum-PSI Team^c

^a UKAEA-CCFE, Culham Science Centre, Abingdon, OX14 3DB, UK

^b Sandia National Laboratories, Albuquerque, NM, 87185, USA

^c DIFFER—Dutch Institute for Fundamental Energy Research, De Zaale 20, 5612 AJ, Eindhoven, Netherlands

ARTICLE INFO

Keywords:

Fusion energy
Plasma facing components
Heat pipes
Lithium
Refractory metals
Thermal radiation

ABSTRACT

In this paper we present results from plasma testing and thermal analysis of a lithium filled tubular heat pipe used as a replaceable plasma facing component (PFC) with no direct cooling. The tantalum envelope (19 mm diameter by 197 mm long) was heated on its side wall using a hydrogen plasma beam in the linear plasma device Magnum-PSI. A single continuous plasma pulse lasting ~2 h was carried out with the isothermal zone of the heat pipe operating at a temperature of ~1000 °C for the whole time with the main heat removal via thermal radiation. Target tilting was used to vary the peak surface heat flux in the range 7.5–13 MW/m². The tilting also increased the magnetic field component normal to the return flow of lithium via the sintered niobium wick to ~0.85 T. Near infra-red thermography was used to measure the surface temperature. Heating power was increased until liquid lithium escaped through a crack in the heat pipe near the beam center. The impact of the lithium leak on the plasma was benign compared to that expected from leaks in helium or water cooled PFCs. The operating limit due to magnetohydrodynamic effects is calculated.

1. Introduction

In 1998 Makhankov [1] described the concept of modular exchangeable plasma facing components (PFCs) based on liquid metal heat pipes which are radiatively cooled. The concept is depicted schematically in Fig. 1. It uses high temperature alkali metal heat pipes as thermal transformers to convert an intense and potentially non-uniform heat flux at one end into a distributed source of thermal radiation spread uniformly over a much larger area. The idea of using heat pipe technology in tokamaks has been around for much longer e.g. Carlson [2] but the innovation in [1] is the suggestion that this technology could be used to make exchangeable plasma facing elements with no direct coolant connection.

2. Benefits of radiatively cooled heat pipes

The main benefit outlined in [1] is that, theoretically at least, failed plasma facing components could be replaced without the need for any cutting or welding of big in-vessel cooling circuits. The small size of the replaceable elements we propose also means maintenance could be carried out by small diameter snake robots on a short timescale

compared to conventional concepts. Significant benefits include:

- The secondary heat exchanger operates at a power density at least 20× lower than that on the heat pipe evaporator and so can be simple/reliable. Heat transfer is almost independent of secondary heat exchanger operating temperature which can be chosen to suit the material.
- The failure mode of a lithium filled heat pipe will be extremely benign compared with that of conventional directly cooled PFC technologies due to low Li inventory.
- The high operating temperature of a Li filled heat pipe (> 900 °C) means that accumulation of hydrogen isotopes is not expected in the Li or heat pipe material and the temperature is optimal with respect to radiation damage resistance for W (a possible pipe material).

3. Experiment strategy

In reference [1], experimental data were presented in which sodium filled heat pipes were tested in the laboratory using a resistive heater at the evaporator end. The heat pipes were 13.8 mm in diameter and

* Corresponding author.

E-mail address: guy.matthews@ukaea.uk (G.F. Matthews).

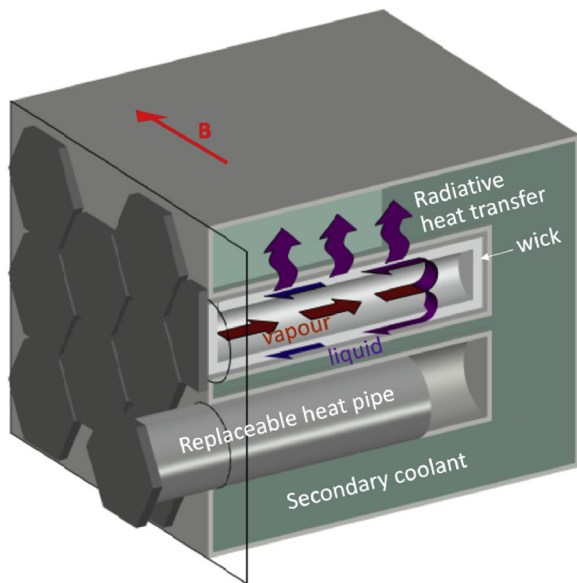


Fig. 1. Concept for high temperature alkali metal heat pipes as modular replaceable high heat flux plasma facing components. Heat is passively redistributed within the pipe via evaporation and condensation of metal vapor and radiated to a secondary heat exchanger. A wide range of geometric variants are possible. Similar sized heat pipes to that shown in Fig. 3 could be used.

450 mm long constructed mainly from niobium. The operating temperature was 650–700 °C and magnetic field up to 1.5 T. Concepts for divertor PFCs are also presented in [1]. In high heat flux areas, higher temperature heat pipes will be required where lithium is the working fluid. Our strategy was to test such a heat pipe in a steady state magnetized hydrogen plasma.

A single legacy tantalum heat pipe (1980s) with lithium fill was procured by Sandia National Laboratories (SNL) [7] from Aavid/Thermacore for testing in the Magnum-PSI linear plasma facility at DIFFER in Eindhoven [3,4]. The heat pipe was not optimized in terms of material or design and so side-wall heating, which is also a potential geometry, had to be used rather than the end heating of Fig. 1. This geometry increases the thermal stresses [7] but the local evaporator heat flow is similar. Our aim was a demonstration rather than optimal performance. Further details of the heat pipe construction are given in [7]. Our goal was to operate at up to 2.8 kW radiated power with the plasma beam offset towards one end to give a heat flow averaged over the 19 mm diameter cross section of $\sim 10 \text{ MW m}^{-2}$. Pebble milling was used to increase the emissivity to 0.6–0.7 (empirical [6]) implying an average heat pipe temperature of $\sim 1250 \text{ °C}$ at the desired power. In practice the maximum total power radiated was $\sim 800 \text{ W}$, Fig. 5(a). It was also not possible to load the heat pipe near one end.

3.1. Magnum-PSI

The linear plasma facility Magnum-PSI is capable of operating at magnetic fields of up to 2.5 T and has achieved beam powers up to 7 kW [3,4]. Enough in theory, to reach the performance limit discussed in Section 5 where magnetohydrodynamic effects limit the liquid Li flow. A section through the target chamber is shown in Fig. 2. The heat pipe was mounted off a water-cooled target holder which could be remotely rotated around the axis of the beam and tilted to change the angle of incidence of the plasma beam on its surface. The heat pipe was mounted clear of the plate between simple supports at either end which were constructed from 0.5 mm molybdenum sheet. The support brackets, visible in Fig. 3, were designed to minimize thermal conduction loss and allow the heat pipe to expand or bow freely.

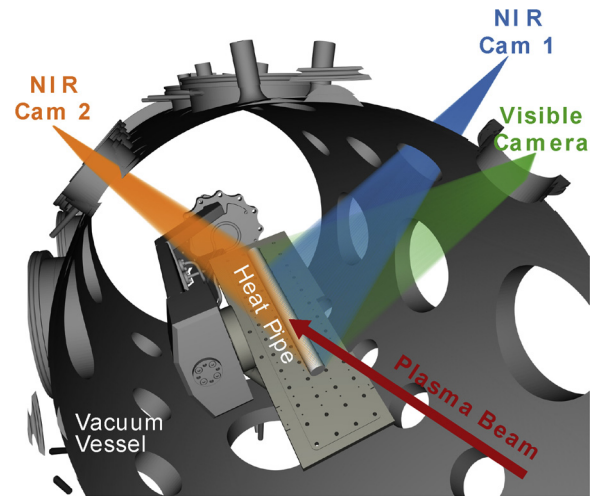


Fig. 2. Target area of Magnum-PSI with camera views [6].

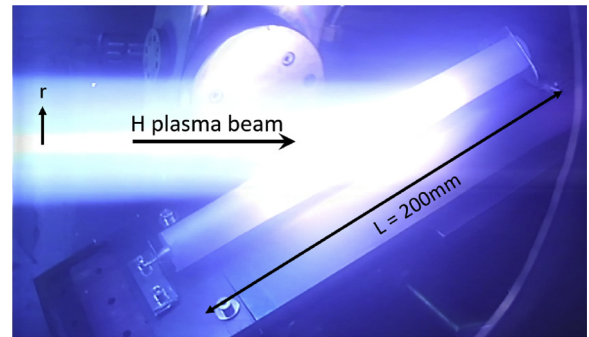


Fig. 3. Visible camera view (target tilted 30° to beam).

Table 1

Experiment sequence and events, total time $\sim 2 \text{ h}$, $B = 1 \text{ T}$. P_C is the total beam power (W) from a calorimeter reference pulse and I_s the plasma source current (A).

hh:mm:ss	Sequence	Tilt θ	I_s	P_C
00:00:00	Beam start	30°	100	1030
00:25:53	Tilt increased	38°	100	1030
00:39:54	Tilt increased	45.5°	100	1030
00:54:00	Tilt increased	58.4°	100	1030
01:06:45	Tilt reduced	30°	100	1030
01:11:37	Power raised	30°	110	1160
01:43:02	Power raised	30°	120	1296
01:43:44	Small Li leak	30°	130	1296
01:56:41	Power raised	30°	130	1500
01:56:58	Large Li leak	30°	120	1500
01:58:06	Reduce power	30°	120	1296
01:58:31	Beam stop	30°	0	0

3.2. Experiment sequence

The magnetic field was set to 1 T for the whole experiment. A single continuous plasma pulse was run which lasted $\sim 2 \text{ h}$. Angle and power scans were carried out as detailed in Table 1 where P_C is the total power from water flow calorimetry in a reference pulse with the heat pipe removed. Total beam power is varied by varying the source current I_s .

The benign failure mode of the heat pipe and post-mortem analysis are described in a companion paper [7]. The likely cause of the failure was grain growth since the Ta material used for the pipe was not grain stabilized.

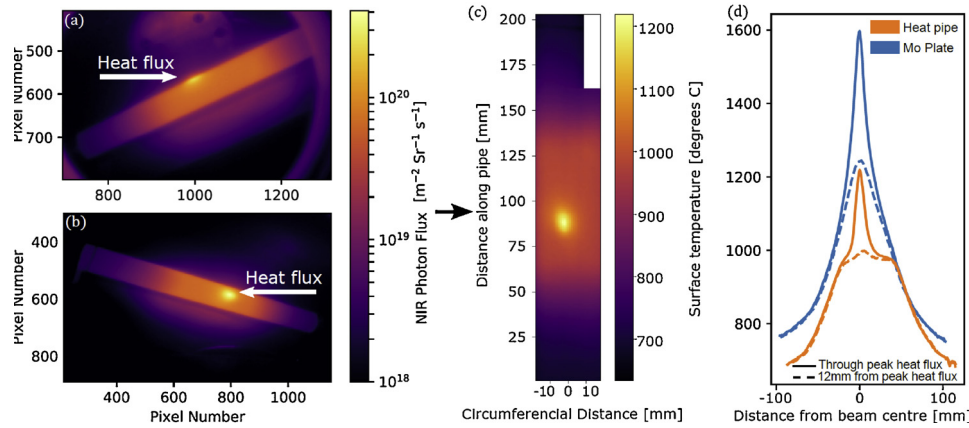


Fig. 4. (a, b) calibrated photon flux images showing the heat pipe under plasma load (616 W) (c) temperature map over the heat pipe surface, (d) 1D profiles along the heat pipe and solid Mo plate targets under identical load.

3.3. Temperature measurements

Thermocouples were not used due to the risk that the available Type K thermocouples would cause failures in the Ta envelope of the heat pipe due to formation of low melting point intermetallic mixtures. The thermal measurement strategy which produced the data in Fig. 4 is described in [6]. It ensures consistency between water flow calorimetry with the heat pipe not in place, NIR measurements of a 2 mm thick Mo plate used as a reference in identical pulses and data from a multi-spectral pyrometer which determines local emissivity and temperature. Although the NIR cameras were absolutely calibrated against a black body source in the laboratory, this procedure was needed to deal with the real emissivity. The uncooled Mo plate reference data provides incident power profiles via ANSYS inverse methods [6], Fig. 5(a). Spatial mapping using CALCAM [5] was used to ensure registration of the NIR cameras with each other and the spectral pyrometer. The appropriate part of the NIR spectrum was then be used to calibrate the emissivity.

4. Results

Parallel power density, which is the power flow along the magnetic field and hence the value for normal incidence ($\theta = 90^\circ$) was derived from the Mo plate reference pulses. Profiles are plotted in Fig. 5(a). The Magnum PSI source current was operated at 100 A, 110 A, 120 A and 130 A with the heat pipe, Mo plate and calorimeter in place in turn. Water flow calorimetry gave the total powers P_C shown in Table 1. Steady state Mo plate data from NIR was processed by inverse ANSYS to give power profiles. At $I_s = 130$ A the Mo plate NIR data saturated so

could not be used. The power density profiles have a narrow intense central peak and a broad halo which is also visible in Fig. 3. Peak powers are consistent with Thompson scattering data from the plasma source, but the profiles become narrow towards the target chamber, Fig. 5(a). The power deposited (P_{HP}) is calculated by mapping these profiles onto the heat pipe geometry using a consistency between the two NIR views to determine point of intersection with the heat pipe, Fig. 4.

Temperature distributions along the heat pipe during the angle and power scans are shown in Figs. 5(b, c). Also plotted are ANSYS forward thermal calculations of the steady state temperature of the radiating heat pipe. The pipe geometry is detailed in reference [7] and the thermal conductivity of the Ta tube and wick are $54 \text{ Wm}^{-1} \text{K}^{-1}$. The vapor space is treated as a high conductivity bar with $10^6 \text{ Wm}^{-1} \text{K}^{-1}$ in the center section and $15 \text{ Wm}^{-1} \text{K}^{-1}$ at the ends with lengths adjusted to match the data. ANSYS shows that the peak temperature near beam centre is consistent with the plate power profiles of Fig. 5(a).

During the tilt scan total power remains constant but peak surface power density rises from $7.5\text{--}13 \text{ MWm}^{-2}$ as expected. The temperature drop in the side wall and wick increases the peak surface temperature but otherwise there is no change. The constant length of the isothermal zone during the tilt scan suggests performance was not limited by magnetic field effects (see next section).

It can be seen in Fig. 4 that the heat pipe was in a transition state not fully iso-thermal. This risked hydrogen accumulation at the ends where $T < 900^\circ \text{C}$. The power was therefore increased stepwise and the isothermal zone expanded, Fig. 5(c). A small transient Li leak was detected retrospectively after the third power step, Table 1, and the final power

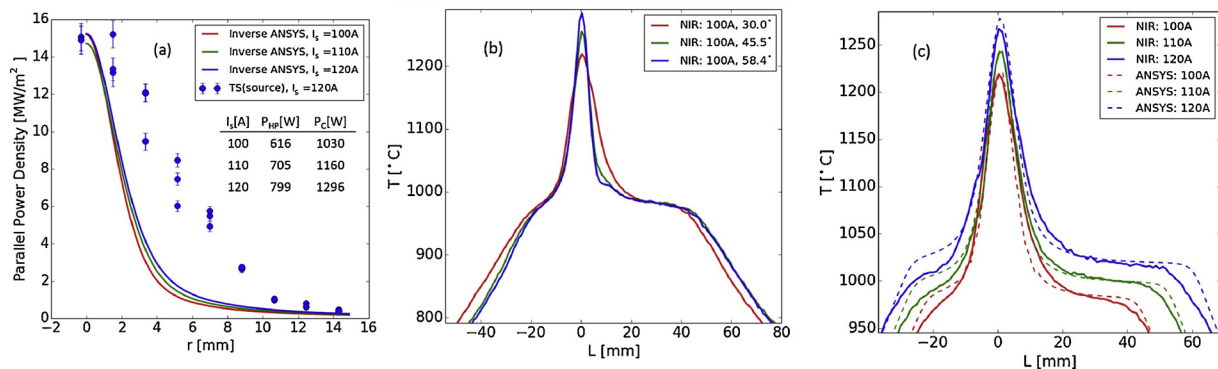


Fig. 5. (a) Beam parallel power density (+18% -9%) at the target derived from inverse ANSYS of the reference pulses using the Mo plate [6] (Fig. 4d). These profiles are made consistent with calorimeter total power P_C and mapped onto the heat pipe to give heat pipe total power PHP. Thompson scattering derived parallel power density at the source for the 120A case is also shown. Fig. 5(b), heat pipe temperature from NIR during the tilt scan ($I_s = 100\text{A}$) and (c) power scan compared with ANSYS heat pipe simulations using the beam parallel power profiles shown in (a) projected onto the heat pipe.

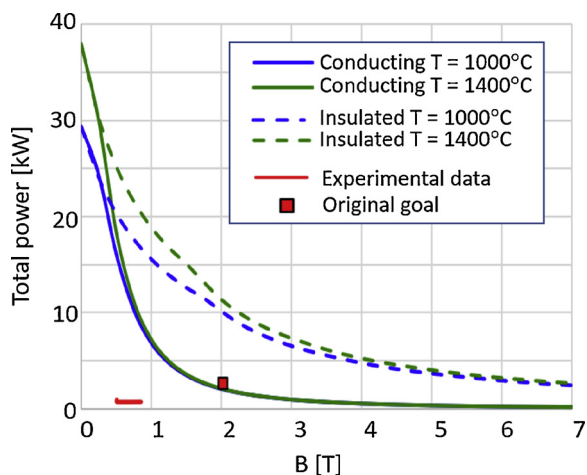


Fig. 6. Capillary limited total power vs magnetic field for conducting and electrically insulated heat pipes from Eq. (1) with geometry as [7]. Our original goal was 2.8 kW.

step created a large Li leak easily visible in the plasma images. The heat pipe kept working until the plasma was stopped and the only operational impact was coated diagnostic windows.

5. Discussion

Even without a magnetic field (B), alkali metal heat pipes have complex operating limits [8]. Critical for fusion applications is the back pressure due to the interaction between induced currents in the liquid lithium and the component of B normal to the flow [9]. The power transported by the Li vapor flow is only limited by the speed of sound [8] and is relatively high and unaffected by B . We have calculated the limit for the power flow in our heat pipe when the capillary pressure is just enough to drive the liquid lithium through the porous medium against viscous and electromagnetic forces. In contrast to [2], we ignore the pressure drop in the vapor space and use recently calculated dimensionless pressure gradients (G_{zz}) based on 3D modelling of a capillary porous system (CPS) for electrically insulating [10] and conducting structures [11] with similar pore radius to ours. Equation 1 gives the total heat pipe power at this limit where d_h is the hydraulic diameter [10], $\rho_L(T)$ [13] is the liquid density, ΔH_{vap} is the latent heat of vaporization, A_w the cross sectional area of the wick, ϵ_p the porosity, P_{cap} is capillary pressure (equation 8 in ref. [2]), $\mu_L(T)$ [13] is the liquid dynamic viscosity and L_{peff} the effective length of the heat pipe (taken to be 0.1 m) in our case.

$$Q_{hp}(B, T) = \frac{d_h^2 \rho_L(T) \Delta H_{vap} A_w \epsilon_p P_{cap}(T)}{\mu_L(T) L_{peff} G_{zz}(B, T)} \quad (1)$$

The results are plotted in Fig. 6 and have the same dependence on B as in [2] but correctly account for the porosity and reduce to the Darcy value at zero field [10]. We have also checked that in strong magnetic fields our normalized pressure gradients match laboratory data [12].

The maximum power we coupled to our heat pipe was 0.8 kW and the maximum component of B normal to the liquid Li flow was 0.85 T.

This puts it well below the capillary limit plotted in Fig. 6. This explains why the isothermal zone is unchanged by the tilt scan, Fig. 5(b).

Consistent with [2] we conclude that even with low electrical conductivity porous wicks, the pressure drop will be too large for high power high field fusion applications and that heat pipes with electrically insulated channel type wicks will be required.

If lithium leaks were to occur inside a fusion reactor then it will be necessary to detect the problem (e.g. via spectroscopy), shutdown the plasma and replace the component. If this is not done, the heat pipe will dry-out and melting may occur. In our experiment the leaking lithium mitigated the plasma heat load which buys time.

6. Conclusions

We have demonstrated operation of a radiatively cooled Ta/Li heat pipe in a magnetized hydrogen plasma in a pulse lasting ~ 2 h. The peak power density exceeded 10 MW m^{-2} at a peak temperature of $\sim 1250^\circ\text{C}$. Total power was $\sim 30\%$ of our goal due to the narrow power profiles obtained in Magnum PSI. The low Li inventory (~ 5 g) meant the failure mode was benign. Materials are the main challenge for fusion application of heat pipes [7] since they determine lifetime at high temperature due to grain growth and H embrittlement. Heat pipe and secondary heat exchanger can each be designed to operate at optimum temperatures to resist neutron damage. To mitigate magnetohydrodynamic pressure losses in the liquid flow Li compatible electrical insulators will have to be developed.

Acknowledgments

The authors would like to thank John Rosenfeld (Aavid/Thermacore) for advice/support during procurement and testing of the heat pipe. Also, we would like to thank Leo Bühler (Karlsruhe Institute of Technology) for advising us on the theory of liquid metal flow through porous media in magnetic fields. This work was part-funded by the RCUK Energy Programme under grant EP/P012450/1. Supported by the US DOE under DE-AC04-94AL85000. DIFFER is part of the Netherlands Organisation for Scientific Research (NWO).

References

- [1] A. Makhankov, *Fusion Eng. Des.* 42 (1998) 373–379.
- [2] G.A. Carlson, M.A. Hoffman, *Transact. ASME* (August) (1972) 282–288.
- [3] G. De Temmerman, et al., *Fusion Eng. Des.* 88 (2013) 483–487.
- [4] H.J.N. van Eck, et al., *Appl. Phys. Lett.* 101 (2012) 224107.
- [5] S.A. Silburn, et al., *Calcam* (2018), <https://doi.org/10.5281/zenodo.1478554>.
- [6] S.A. Silburn, et al., *Proc. 45th European Physical Society Conference on Plasma Physics, Europhysics Conference Abstracts 42A*, (2018) P5.1008.
- [7] R. Nygren, SOFT 2018 Post-test Examination of a Li-Ta Heat Pipe Exposed to H Plasma in Magnum-PSI, (2018).
- [8] A. Faghri, *Heat Pipe Science and Technology*, Global Digital Press, 2016.
- [9] U. Müller, L. Bühler, *Magnetofluidynamics in Channels and Containers*, Springer, 2001.
- [10] L. Bühler, C. Mistrangelo, T. Najuch, *Fusion Eng. Des.* 98–99 (2015) 1239–1243.
- [11] T. Najuch, Diploma Thesis, Numerical Simulation of Liquid Metal Flows through Porous Structures in Strong Magnetic Fields, Karlsruhe Institute of Technology - University of the State of Baden-Wuerttemberg, 2014.
- [12] J.D. McWhirter, et al., *Fusion Technol.* 34 (1998) 187–197.
- [13] NASA TN D-4650 by H.W. Davison, (1968).